Towards Regional Assimilation of Lagrangian Data: The Lagrangian Form of the Shallow Water Model and its Inverse

J.L. Mead *
Department of Mathematics and Computer Science
Boise State University
Boise, ID 83725 USA
Tel 208 426-2432, Fax 208 426-1356
* corresponding author, mead@math.boisestate.edu
and
A.F. Bennett †
Office of Naval Research Science Unit
Fleet Numerical Meteorology and Oceanography Center
Monterey CA 93943-5501 USA
Tel 831 656-4484, Fax 831 656-4703
† bennetta@fnmoc.navy.mil

October 12, 2000

Abstract

Variational data assimilation for Lagrangian geophysical fluid dynamics is introduced. Lagrangian coordinates add numerical difficulties into an already difficult subject, but also offer certain distinct advantages over Eulerian coordinates. First, float position and depth are defined by linear measurement functionals. Second, Lagrangian or 'comoving' open domains are conveniently expressed in Lagrangian coordinates. The attraction of such open domains

is that they lead to well-posed prediction problems [Bennett and Chua, (1999)] and hence efficient inversion algorithms.

Eulerian and Lagrangian solutions of the inviscid forward problem in a doubly periodic domain, with North Atlantic mesoscales, are compared and found to be in satisfactory agreement for about one day. Viscous stresses vastly extend the interval of agreement at the cost of considerable complexity, so in this first study the machinery of variational assimilation is developed and tested for inviscid dynamics, simulated data and short assimilation intervals. It was found that the intricate machinery could be consistently developed, managed, and satisfactorily tested at least within the confines of the chosen parameters.

1 Introduction

Data assimilation combines a model and data in order to get the best estimate of the state of the ocean. "Best" is defined here in the weighted least squares sense. In principle, the data compensate for poorly known information, such as boundary values, initial conditions, and parameterizations.

Lagrangian data are increasingly becoming available. Expressing the dynamics of the model in Lagrangian coordinates, rather than Eulerian coordinates, offers distinct advantages and disadvantages. Here we take first steps towards variational assimilation of Lagrangian data into a Lagrangian model. The data are simulated float trajectories on an isopycnal surface, while the dynamics are those of the inviscid shallow water equations. The scales of the simulated fields are those of the mesoscale or eddy variability in the western North Atlantic.

One of the difficulties with Lagrangian data and Lagrangian models is that 'Lagrangian chaos' can occur. For example, recent float deployments have shown that floats released in neighboring pairs or triplets can have drastically different trajectories [Rossby et al., (1999)]. Detailed discussions on chaos in Lagrangian motion can be found in [Aref, (1984)], [Samelson, (1996)], and [Yang and Liu, (1996)]. A consequence of this chaos is that for long integration times, particle positions can become sensitive to initial conditions, forcings and errors in parameterizations. Thus it is important to use data assimilation in order to keep the solution realistic.

Assimilation of drifter data into a primitive equation model, for prediction of particle trajectories, was reported in [Özgökmen et al., (1999)]. They conclude that if there is 1 particle per a $0.25^\circ \times 0.25^\circ$ region, accurate predictions can be obtained for one week to three months, depending on the region. They also note that prediction error increases with time, most likely due to the above mentioned chaotic behavior of Lagrangian motion. Of course, shear leads to loss of predictability in Eulerian models too, but Lagrangian models do offer one highly significant advantage. They naturally facilitate the formulation and integration of regional models, when the domain is moving with the flow, or 'comoving' [Bennett and Chua, (1999)]. A few explanatory remarks are in order.

In the open ocean, the Eulerian form of the primitive equations is ill-posed as an initial-boundary value problem [Oliger and Sundström, (1978)], unless the boundary conditions are applied mode by mode in the vertical direction. The problem occurs if particle speeds lie within the range of phase speeds of internal gravity wave modes, because the flow is variously supercritical and subcritical, according to which mode is involved. It therefore becomes impossible

to ascribe the correct number of *vertically local* boundary conditions at each vertical level.

However, the generalized inverse problem for the primitive equation model is well posed in the open ocean [Bennett, (1992)]. The best fit, in a weighted least squares sense, of the data, the model and local boundary values for all fields at all levels is governed by variational or Euler-Lagrange equations, and they form a well-posed two point boundary value problem in time.

The linearized Euler-Lagrange equations can not be solved by a finite number of backward integrations and forward integrations, because they are ill-posed (since the forward primitive equation model is ill-posed). However, the solution of the linear or nonlinear Euler-Lagrange equations is the minimum of a cost functional, and the minimum (extremum) can be found by direct substitution methods such as gradient decent, random walk and hybrid Monte Carlo searches [Bennett and Chua, (1994)].

As mentioned, it has recently been shown [Bennett and Chua, (1999)] that the initial boundary value problem for the inviscid primitive equation model is well posed if its open boundaries are fluid particles, that is, if they are moving with the flow or are 'comoving' . Since vorticity is conserved on fluid particles, vorticity cannot advect into or out of the domain. Divergence can radiate into or out of the domain as gravity wave propagation, and every mode is subcritical in the reference frame of the moving boundary. In the vertical, the boundary conditions do not need to be applied mode by mode. It is particularly convenient to express the equations of motion in Lagrangian coordinates when the domain boundary is comoving. In addition, assimilation of Lagrangian data such as location, temperature and salinity, into a model represented

in Lagrangian coordinates, leads to *linear* measurement functionals.

In summary, the increasing availability of Lagrangian data, the well-posedness of inviscid primitive equation models in comoving domains, and the linearity of measurement functionals from float data prompt us to take steps in the task of variational assimilation of Lagrangian data into a prototype of the invsicid primitive equations in a comoving domain. This prototype consists of the shallow water equations.

In Section 2 we will state the Lagrangian form of the shallow water model and compare it to the Eulerian form. In Section 3 we will give the inverse of the Lagrangian formulation, and in Section 4 we will give results from a short-term inversion with synthetic data and inviscid dynamics.

2 Lagrangian formulation of the dynamical model

2.1 Dynamics: models and scales

Let λ be the longitude, and θ the latitude of a particle. If r is the earth's radius, the zonal and meridional velocities on the sphere are defined by

$$u = r\cos\theta\frac{D\lambda}{Dt}, \quad v = r\frac{D\theta}{Dt}, \tag{1}$$

where $\frac{D}{Dt}$ is a material derivative, following the motion. The Eulerian form of the momentum equations in the shallow water model is

$$\frac{D\boldsymbol{u}}{Dt} + \hat{\boldsymbol{k}} \times \left(\frac{u}{r}\tan\theta + 2\Omega\sin\theta\right)\boldsymbol{u} = -g\boldsymbol{\nabla}h \tag{2}$$

or

$$\frac{Du}{Dt} - \left(\frac{u}{r}\tan\theta + 2\Omega\sin\theta\right)v = -\frac{g}{r\cos\theta}\frac{\partial h}{\partial\lambda} \quad (3)$$

$$\frac{Dv}{Dt} + \left(\frac{u}{r}\tan\theta + 2\Omega\sin\theta\right)u = -\frac{g}{r}\frac{\partial h}{\partial\theta} \quad (4)$$

where h is the equivalent depth, g the mean gravitational acceleration, and Ω the angular sidereal rotation rate of the earth [Gill, (1982)]. The total material derivative on time following the motion is

$$\frac{D}{Dt} = \frac{\partial}{\partial t} + \frac{u}{r\cos\theta}\frac{\partial}{\partial\lambda} + \frac{v}{r}\frac{\partial}{\partial\theta}. \quad (5)$$

The continuity equation is

$$\frac{Dh}{Dt} + h\boldsymbol{\nabla}\cdot\mathbf{u} = 0. \quad (6)$$

or

$$\frac{\partial h}{\partial t} + \frac{1}{r\cos\theta}\left[\frac{\partial}{\partial\lambda}(hu) + \frac{\partial}{\partial\theta}(hv\cos\theta)\right] = 0 \quad (7)$$

In the Eulerian form, we use as independent variables the position (λ,θ), and we solve for the particle velocities u, v and depth h as dependent variables at time t. In the Lagrangian form, we use as independent variables the initial particle position (α,β), and we solve for the subsequent particle position (λ, θ) and depth h as dependent variables at time t. The first form describes the evolution observed at points fixed in space, while the second form is the evolution that would be observed as we follow the motion of particles.

The change in coordinates from (λ, θ, t) to (α, β, t) is performed using (1) and the transformation

$$\boldsymbol{u}(\lambda,\theta,t) \Longrightarrow \boldsymbol{u}(\lambda(\alpha,\beta,t),\theta(\alpha,\beta,t),t). \tag{8}$$

The Eulerian partial derivatives of h, for example, are related its Lagrangian partial derivatives by

$$\frac{\partial h}{\partial \lambda} = J^{-1}\left(\frac{\partial h}{\partial \alpha}\frac{\partial \theta}{\partial \beta} - \frac{\partial \theta}{\partial \alpha}\frac{\partial h}{\partial \beta}\right), \tag{9}$$

$$\frac{\partial h}{\partial \theta} = J^{-1}\left(\frac{\partial \lambda}{\partial \alpha}\frac{\partial h}{\partial \beta} - \frac{\partial \lambda}{\partial \beta}\frac{\partial h}{\partial \alpha}\right) \tag{10}$$

where the Jacobian of the transformation is

$$J = \frac{\partial \lambda}{\partial \alpha}\frac{\partial \theta}{\partial \beta} - \frac{\partial \lambda}{\partial \beta}\frac{\partial \theta}{\partial \alpha}.$$

Conservation of momentum on the rotating sphere is expressed in Lagrangian coordinates as

$$\frac{\partial^2 \lambda}{\partial t^2} - \left(2\frac{\partial \lambda}{\partial t} + 2\Omega\right)\frac{\partial \theta}{\partial t}\tan\theta = \frac{-g}{(r\cos\theta)^2}J^{-1}\left(\frac{\partial h}{\partial \alpha}\frac{\partial \theta}{\partial \beta} - \frac{\partial \theta}{\partial \alpha}\frac{\partial h}{\partial \beta}\right) \tag{11}$$

$$\frac{\partial^2 \theta}{\partial t^2} + \left(\frac{\partial \lambda}{\partial t} + 2\Omega\right)\frac{\partial \theta}{\partial t}\sin\theta\cos\theta = \frac{-g}{r^2}J^{-1}\left(\frac{\partial \lambda}{\partial \alpha}\frac{\partial h}{\partial \beta} - \frac{\partial h}{\partial \alpha}\frac{\partial \lambda}{\partial \beta}\right), \tag{12}$$

while conservation of volume becomes

$$\frac{\partial (h\cos\theta J)}{\partial t} = 0. \tag{13}$$

Note that the partial derivatives in (11)-(13), with respect to t, are for fixed initial particle position (α, β).

The region of interest here is that of the North Atlantic Current project [Anderson et al., (1996)]; it extends from 35° North to 55° North and from 55° West to 30° West. In this region, the deformation radius is approximately 20 km, and phase speeds c are 2 m/s [Chelton et al., (1998)]. We shall not use the real float data available in that region [Anderson et al., (1996)] in this first study, but we shall use simulated fields with these scales.

2.2 Numerics

The essential computational problem with (11)-(13) is that the Lagrangian strains $\frac{\partial\lambda}{\partial\alpha}$, $\frac{\partial\lambda}{\partial\beta}$, $\frac{\partial\theta}{\partial\alpha}$, $\frac{\partial\theta}{\partial\beta}$ can become increasingly large, as neighboring fluid particles move further and further apart. There is little published experience with the numerics for the Lagrangian form of the shallow water model. Semi-Lagrangian methods are widely used [Staniforth and Côté, (1991)] to improve the efficiency of numerical weather prediction models. The Lagrangian form of advection is used to advance the velocities; however, the trajectories of the particles are interpolated on to the Eulerian grid at the current time. When assimilating float data, it is unattractive to interpolate to an Eulerian grid, as any such interpolation introduces error. Thus we shall experiment first with fully Lagrangian integrations, and keep semi-Lagrangian methods as an alternative for later consideration.

Dissipation must eventually be added to (3)-(7), otherwise the system becomes unstable owing to a turbulent cascade to the maximum resolved wave number (the particle velocities can violate the Courant-Friedrichs-Lewy condition, and in addition, the depths can become negative, in which case the numerical gravity wave dynamics become elliptic e.g.,

[Bennett and Middleton, (1983)]). With a deformation radius of 20 km and phase speeds of 2 m/s, parameters corresponding to those in the North Atlantic, we found that the Lagrangian form (11)-(13) became unstable a couple of days before the Eulerian form, indicating that the Lagrangian numerics can be more sensitive. Once friction is added to both the Eulerian form and the Lagrangian form with a grid Reynolds number (fluid speed $\times$ longitudinal grid spacing $\div$ viscosity) [Bennett and Middleton, (1983)] equal to 1, both methods are stable for at least 100 days. It may be argued that including dissipation resolves the ill-posedness of the Eulerian problem, eliminating the need for the Lagrangian domain. We argue that it would in general do so by fitting discontinuities with spurious viscous boundary layers. We wish to resolve the ill-posedness of the underlying inviscid problem, by correct choice of the domain and boundary conditions. Therefore, in this preliminary study, we will only assimilate data for a few hours and without friction. It must also be conceded that rigorous inclusion of viscous effects in (11)-(13) leads to great complications.

Initially, we choose simple numerics, although more work needs to be done for accurate numerical integration of (11)-(13). We used centered second order finite difference approximations on the A grid [Arakawa, (1966)] with no filtering. To compensate for the low order of the numerics, and the threat of rapidly growing shears $\frac{\partial \lambda}{\partial \alpha}$ etc., 20 points per wavelength were used in the spatial approximation. These calculations were performed on the CM5 and CM500e Connection Machines at the College of Oceanic and Atmospheric Sciences, Oregon State University.

2.3 Numerical test problem

The test problem uses boundary and initial conditions for a combination of plane waves of small amplitude, or Sverdrup waves [Gill, (1982)]. The combination solves the linear form of (3)-(7) exactly, and is given by

$$u = -2\sin(\delta - \omega t)\frac{g\hat{H}}{\omega^2 - f^2}\left[\frac{(72/5)k\omega}{r\cos\theta}\sin(\gamma) - \frac{(72/4)lf}{r}\cos(\gamma)\right] \tag{14}$$

$$v = 2\cos(\delta - \omega t)\frac{g\hat{H}}{\omega^2 - f^2}\left[\frac{(72/4)l\omega}{r}\cos(\gamma) + \frac{(72/5)kf}{r\cos\theta}\sin(\gamma)\right] \tag{15}$$

$$h = H + 2\cos(\gamma)\cos(\delta - \omega t)\hat{H}, \tag{16}$$

$$\omega^2 = f^2 + c^2\left[\left(\frac{72k/5}{r\cos\theta}\right)^2 + \left(\frac{72l/4}{r}\right)^2\right].$$

Here c is the phase speed, $H = c^2/g$ the mean depth, $\hat{H} = \epsilon H$, $\epsilon = .01$, and $f = 2\Omega\sin\theta$ the Coriolis parameter. Since the deformation radius is 20 km, we choose a longitudinal wave number $k = 22$ per radian of longitude, and a latitudinal wave number $l = 18$ per radian of latitude. In addition

$$\gamma = k(72\lambda/5 + 22\pi/5) \tag{17}$$

$$\delta = l(72\theta/4 - 7\pi/2). \tag{18}$$

These give spatially periodic initial conditions in the interval of interest.

The meridional velocities range from $-.04$m/s to .04 m/s, and the zonal velocities range from $-.03$m/s to .03 m/s. The equivalent depth, h, ranges between .402m and .416 m. The initial conditions are plotted in Figure 1 to illustrate these properties.

At a Lagrangian open boundary, the correct open boundary conditions are; the equivalent depth at each boundary, the current latitude at each point on the North and South boundaries, and the current longitude at each point on the East and West boundaries [Bennett and Chua, (1999)]. However, the equivalent boundary conditions at an Eulerian open boundary, i.e. specifying equivalent depth at each boundary, u at East and West, and v at North and South lead, in general, to an ill-posed problem. Since periodic boundary conditions in periodic Lagrangian and Eulerian coordinates lead to well-posed problems in both forms, they were used in this experiment.

There were 440 grid points in the horizontal direction, 360 in the vertical, and the time step was 500 seconds.

After integrating for one day, the waves had traveled approximately three wavelengths. The path that one particle (or float) took during this day is the dependent variable in the Lagrangian form, and is plotted in Figure 2. We see here how solutions of the Lagrangian form simulate trajectories; and in this case, the trajectories are open loops since the dynamics are nonlinear. All particles in the domain behave similarly.

The total distance each particle traveled from its initial position, is plotted in Figure 3. There are $440 \times 360 = 158,400$ particles, and in order to distinguish them in the Figure, only 1/7 of them are plotted. The symmetry of the patterns is due to the periodic initial conditions and boundary conditions. After one day, some particles may have returned to a position near their initial position. Nevertheless, the path they took is much larger than their distance from their initial position, as evidenced by Figure 2.

The initial domain is an open rectangular region, and in the Lagrangian form, it distorts with time. After one day, there is only a small distortion of the domain, and the Lagrangian grid still appears rectangular. In Figure 2 we see that the largest distance a particle has moved is 400 m latitudinally and 600 m longitudinally, which is not noticeable in a domain of approximate width 3000 km and length 2000 km.

We also illustrate the computational difficulties with the increasing Lagrangian strains $\frac{\partial\lambda}{\partial\alpha}$, $\frac{\partial\lambda}{\partial\beta}$, $\frac{\partial\theta}{\partial\alpha}$, $\frac{\partial\theta}{\partial\beta}$ in Figure 4. They are each plotted vs. time for a period of 5 days. Initially $\frac{\partial\lambda}{\partial\alpha} = \frac{\partial\theta}{\partial\beta} = 1$, and $\frac{\partial\lambda}{\partial\beta} = \frac{\partial\theta}{\partial\alpha} = 0$. The strains oscillate initially, as we would expect from the initial conditions (14)-(18). After 5 days the strains increase by an amount of $O(10^{-2})$, and as they continue to increase, the right hand side of (11)-(12) will become large, and the computations eventually become unstable.

Since solutions of the differential equations degrade with time, their accuracy is assessed at the final integration time. The exact solution of the nonlinear equation is not known, so the accuracy of the solution of the Lagrangian form was determined by comparing it to solutions of the Eulerian form. In order to compare the two forms, the velocities and depth found on the distorted Lagrangian grid were interpolated to the Eulerian grid using the function 'griddata' in Matlab. We choose the option 'linear' which uses Delaunay triangularization to create a triangular grid for the scattered data. Then the data are fit to a locally linear surface.

The difference between the two solutions is plotted in Figure 5; including the equivalent depth, meridonal and zonal velocities. The displacement in equivalent depth is approximately $2\hat{H}$, thus the Lagrangian solution differs from the Eulerian solution by about $2 \times 10^{-4}/8.17 \times$

$10^{-3} = 2.5\%$, and similarly for the velocities.

3 Inverse Formulation

The example in Section 2.3 indicates that the Lagrangian form of the shallow water model, without friction, may be numerically integrated with good accuracy for time periods up to one day, when the initial and boundary data have scales of North Atlantic eddy variability. In this section, we will describe the assimilation method, and in Section 4 we will assimilate a few hours worth of simulated data. We realize that longer assimilations are needed, with months of data. It will accordingly be necessary to include friction which greatly complicates the Lagrangian form. The diffusive term $\nabla^2 u$ in Eulerian coordinates becomes

$$r \cos\theta_0 \left\{ \frac{1}{r^2 \cos^2\theta_0} J^{-1} \frac{\partial(L,\theta)}{\partial(\alpha,\beta)} + \frac{1}{r^2} J^{-1} \frac{\partial(\lambda, M)}{\partial(\alpha,\beta)} \right\},$$

where

$$L = J^{-1} \frac{\partial(\lambda_t, \theta)}{\partial(\alpha,\beta)} \quad M = J^{-1} \frac{\partial(\lambda, \lambda_t)}{\partial(\alpha,\beta)},$$

on a flat earth in Lagrangian coordinates. Therefore, we decided first to verify that it is possible to solve the Euler-Lagrange equations for variational assimilation with respect to the inviscid Lagrangian reduced gravity shallow water model.

The generalized inverse, or best fit of the model and data, may be obtained using the calculus of variations. This leads, as indicated, to an Euler-Lagrange system which in turn can be solved using the representer method [Bennett, (1992)]. This method is based on the assumption that the model and the measurement functionals are linear, but it may be applied iteratively to

nonlinear problems [Bennett, (1992)].

As mentioned in the Introduction, the measurement operators for float depth and position are linear in the Lagrangian form. However, the model is highly nonlinear, since the pressure gradient term involves an inverse jacobian, and products of partial derivatives. In order to overcome this difficulty, we define the tangent linearization of the model, derive the associated linear Euler-Lagrange equations, solve the latter by the representer method, and iterate. This approach is described in detail in [Ngodock et al., (1999)] for an Eulerian model with Eulerian (moored) data.

3.1 Iterative tangent linear model

Let $\boldsymbol{\lambda} = [\ \lambda \quad \theta\ ]^{\mathrm{T}}$ and $\boldsymbol{\alpha} = [\ \alpha \quad \beta\ ]^{\mathrm{T}}$ (the superscript T denotes transposition), and linearize (11)-(13) about a previous iterate. That is, given values of $\boldsymbol{\lambda}$ and h at all points in space $\boldsymbol{\alpha}$ and time t for the $(n-1)$st iterate, we find them at the nth iterate by solving the linear equations

$$\frac{\partial^2 \boldsymbol{\lambda}^n}{\partial t^2}(\boldsymbol{\alpha}, t) = \mathbf{L}^{n-1}\boldsymbol{\lambda}^n(\boldsymbol{\alpha}, t) + \boldsymbol{g}_1{}^{n-1} \tag{19}$$

$$h^n(\boldsymbol{\alpha}, t) = \mathrm{l}^{n-1} \cdot \boldsymbol{\lambda}^n(\boldsymbol{\alpha}, t) + g_2{}^{n-1}. \tag{20}$$

The matrix $\mathbf{L}^{n-1}$, vectors l^{n-1} and $\boldsymbol{g}_1{}^{n-1}$, and $g_2{}^{n-1}$ are all functions of $\boldsymbol{\lambda}^{n-1}$, and the partial derivative operators $\partial/\partial\alpha$, $\partial/\partial\beta$, $\partial/\partial t$, $\partial^2/\partial\alpha\partial\beta$, $\partial^2/\partial\alpha^2$ and $\partial^2/\partial\beta^2$. Explicit expressions are given in appendix A, including an equivalent vector form more amenable to programming. Note that n is *not* a time index, but an index for functional iteration.

In Figure 6, we plot the latitude, longitude and equivalent depth of one particle, or float, over a time period of a few hours. An initial guess or background (e.g. λ^0) is needed to begin the

iterations. In this experiment, ϵ (as in section 2.3) was chosen to be 0.1, but for the background, $\epsilon = 0.01$. Thus the background solution is slower than the solution from the nonlinear model. In addition, the location of the float in the background is the same as that from the nonlinear solution initially, however, the equivalent depth is different. The background values for $\boldsymbol{\lambda}$ and h, at each time step, are plotted along side solutions of (19)-(20) for the first three iterations.

By the second iteration, solutions of the linear model converge to the nonlinear model. In fact, solutions in the third iteration are indistinguishable from the second; for all of h, λ, and θ. Figure (7) shows similar plots, but for the average of h, λ, and θ over the entire domain. The convergence occurs by the second iterate in all cases. Slower convergence is expected for longer integration times.

Results from this experiment indicate that given a background solution near the nonlinear solution, iterations on the tangent forward linear model converge to the nonlinear solution. Had this not been the case, we would have little encouragement for proceeding with the nonlinear Euler-Lagrange or adjoint equations. In the inversion, the background is taken to be the solution of the forward nonlinear problem.

3.2 Iterative inverse problem statement

In general, we shall assume there are errors in the model, and thus will only allow the model to act as a weak constraint. However, in order to simplify the Jacobian terms in (11) and (12) in this preliminary study, we have substituted the solution of (13): $h = (J\cos\theta)^{-1}h(\boldsymbol{\alpha},0)\cos(\theta(\boldsymbol{\alpha},0))$ (note here that $J(\boldsymbol{\alpha},0) = 1$). This means we are assuming that there are no errors in the

continuity equation, nor in the initial condition for h.

Let

$$\boldsymbol{f}^{\lambda} = [\ f^{\lambda} \quad f^{\theta}\ ], \qquad \boldsymbol{i} = [\ i^{\lambda_t} \quad i^{\theta_t}\ ], \tag{21}$$

$$\boldsymbol{b}^{\lambda} = [\ b^{\lambda_w} \quad b^{\lambda_e} \quad b^{\theta_s} \quad b^{\theta_n}\ ], \quad \boldsymbol{b}^{h} = [\ b^{h_w} \quad b^{h_e} \quad b^{h_s} \quad b^{h_n}\ ], \tag{22}$$

$$\boldsymbol{\epsilon}^{\lambda} = [\ \epsilon_1^{\lambda} \quad \ldots \quad \epsilon_M^{\lambda} \quad \epsilon_1^{\theta} \quad \ldots \quad \epsilon_M^{\theta}\ ], \qquad \boldsymbol{\epsilon}^{h} = [\ \epsilon_1^{h} \quad \ldots \quad \epsilon_M^{h}\ ], \tag{23}$$

be the errors in the dynamics, velocity initial conditions, boundary conditions, and data respectively. That is, we replace (19) with

$$\frac{\partial^2 \boldsymbol{\lambda}^n}{\partial t^2} = \mathbf{L}^{n-1}\boldsymbol{\lambda}^n + \boldsymbol{g}_1{}^{n-1} + \boldsymbol{f}^{\lambda} \tag{24}$$

and

$$h^n = \mathbf{l}^{n-1} \cdot \boldsymbol{\lambda}^n + g_2{}^{n-1}, \tag{25}$$

is the same as (20). The initial conditions are

$$\boldsymbol{\lambda}^n(\boldsymbol{\alpha}, 0) = \boldsymbol{\alpha} \tag{26}$$

$$\frac{\partial}{\partial t}\boldsymbol{\lambda}^n(\boldsymbol{\alpha}, 0) = \boldsymbol{u}^I + \boldsymbol{i} \tag{27}$$

$$h^n(\boldsymbol{\alpha}, 0) = h^I, \tag{28}$$

for given initial position $\boldsymbol{\alpha}$, velocity $\boldsymbol{u}^I = [\ u^I \quad v^I\ ]^{\mathrm{T}}$, and depth h^I. The boundary conditions are

$$\boldsymbol{\lambda}^n \cdot \boldsymbol{n}_r = \lambda_r^B + b^{\lambda_r} \tag{29}$$

$$h_r^n = h_r^B + b^{h_r}, \tag{30}$$

for given current latitude or longitude λ_r^B, and depth h_r^B at the boundary. Here r is an index (n, s, e, w) that represents either the north, south, east, or west boundary, and $\boldsymbol{n}_r$ is the unit normal vector in the corresponding direction.

A generic notation like that of [Ide et al., (1997)] is useful for general discussion; however, we wish to expose the Lagrangian detail here. Later, it could be mapped into generic notation.

Assume we are given the longitude, latitude and equivalent depth of a float on an isopycnal as data. Then the data are direct measurements of the fields in the Lagrangian form. Let M' be the number of times data are taken from the floats (e.g. if 5 floats record data 2 times each, then $M' = 10$). Denote the location of the float $\boldsymbol{d}^\lambda$, and the depth of the float by d^h. Then for $1 \leq m \leq M'$

$$\boldsymbol{d}_m^\lambda = \boldsymbol{\lambda}(\boldsymbol{\alpha}_m, t_m) + \boldsymbol{\epsilon}_m^\lambda \tag{31}$$

$$d_m^h = h(\boldsymbol{\alpha}_m, t_m) + \epsilon_m^h, \tag{32}$$

where $\boldsymbol{\epsilon}_m^\lambda$ and ϵ_m^h are the errors in the mth datum point. Note that the total number of data is $M{=}3M'$, and $\boldsymbol{\alpha}_m$ is the initial position of the float from which the mth data point was taken at time t_m.

At each iterate 'n', we minimize the cost functional

$$\begin{aligned} J[\boldsymbol{\lambda}^n] = {} & \boldsymbol{W}_{f^\lambda} \cdot \int_0^T dt \int_{\mathcal{B}} d\boldsymbol{\alpha} (\boldsymbol{f}^\lambda)^2 + \boldsymbol{W}_i \cdot \int_{\mathcal{B}} (\mathbf{i})^2 d\boldsymbol{\alpha} + \boldsymbol{W}_b \cdot \int_0^T (\mathbf{b}^\lambda)^2 dt \\ & + \boldsymbol{W}_h \cdot \int_0^T (\mathbf{b}^h)^2 dt + \omega^\lambda \sum_{m=1}^M (\epsilon_m{}^\lambda)^2 + \omega^\theta \sum_{m=1}^M (\epsilon_m{}^\theta)^2 + \omega^h \sum_{m=1}^M (\epsilon_m{}^h)^2 \end{aligned} \tag{33}$$

subject to (25), using the calculus of variations. Here $\boldsymbol{W}_{f^\lambda}$, $\boldsymbol{W}_i$, $\boldsymbol{W}_b$, $\boldsymbol{W}_h$, $\boldsymbol{\omega}^\lambda$, and ω^h are prescribed weights for the errors in the momentum equations, initial conditions, boundary con-

ditions and data. In this first study, we assume that $\boldsymbol{f}^{\lambda}$ etc., are uniform white noise in space and time. That is, the weighting is homogeneous and 'diagonal'.

3.3 Euler-Lagrange equations

From now on, the iteration subscripts n and $n-1$ are omitted. The optimal solutions $\hat{\boldsymbol{\lambda}}$ and $\hat{h}$ minimize (33) and satisfy the Euler-Lagrange equations

$$\frac{\partial^2 \boldsymbol{\lambda}^A}{\partial t^2} = \mathbf{L}^A \boldsymbol{\lambda}^A - \sum_{m=1}^{M} \boldsymbol{\omega}^{\lambda}(\boldsymbol{d}_m^{\lambda} - \hat{\boldsymbol{\lambda}}(\boldsymbol{\alpha}_m, t_m))\delta(\boldsymbol{\alpha} - \boldsymbol{\alpha}_m)\delta(t - t_m) \tag{34}$$

$$\zeta = \mathrm{l}^A \cdot \boldsymbol{\lambda}^A - \sum_{m=1}^{M} \omega^h(d_m^h - \hat{h}(\boldsymbol{\alpha}_m, t_m))\delta(\boldsymbol{\alpha} - \boldsymbol{\alpha}_m)\delta(t - t_m) \tag{35}$$

where $\boldsymbol{\lambda}^A$ is the adjoint variable corresponding to $\boldsymbol{\lambda}$, and $\mathbf{L}^A$ and l^A are time-dependent adjoint operators corresponding to $\mathbf{L}$ and l respectively. Definitions are given in Appendix B. In addition, ζ is the Lagrange multiplier which enforces (25) as a strong constraint.

The adjoint equations (34)-(35) are subject to the terminal conditions:

$$\boldsymbol{\lambda}^A(\boldsymbol{\alpha}, T) = 0 \tag{36}$$

$$\frac{\partial \boldsymbol{\lambda}^A}{\partial t}(\boldsymbol{\alpha}, T) = 0 \tag{37}$$

$$\zeta(\boldsymbol{\alpha}, T) = 0. \tag{38}$$

Now $\hat{\boldsymbol{\lambda}}$ and $\hat{h}$ in (34) and (35) satisfy

$$\frac{\partial^2 \hat{\boldsymbol{\lambda}}}{\partial t^2} = \mathbf{L}\hat{\boldsymbol{\lambda}} + \boldsymbol{g}_1 + \mathbf{W}_{f^{\lambda}}^{-1} \boldsymbol{\lambda}^A \tag{39}$$

$$\hat{h} = \mathrm{l} \cdot \hat{\boldsymbol{\lambda}} + g_2, \tag{40}$$

with initial conditions

$$\hat{\boldsymbol{\lambda}} = \boldsymbol{\alpha} \tag{41}$$

$$\frac{\partial \hat{\boldsymbol{\lambda}}}{\partial t} = \boldsymbol{u}^I + \mathbf{W}_i^{-1} \boldsymbol{\lambda}^A \tag{42}$$

$$\hat{h}^n = h^I, \tag{43}$$

and boundary conditions

$$\hat{\boldsymbol{\lambda}} \cdot \boldsymbol{n}_r = \lambda_r^B + \mathbf{W}_b^{-1} \mathbf{p}(\mathbf{L}^A, \boldsymbol{\lambda}^A, \zeta) \tag{44}$$

$$\hat{h}_r = h_r^B + \mathbf{W}_h^{-1} \cdot \mathbf{q}(\mathbf{L}^A, \boldsymbol{\lambda}^A). \tag{45}$$

Definitions of $\mathbf{p}$ and $\mathbf{q}$ are also given in Appendix B.

Note that in order to solve for $\hat{\boldsymbol{\lambda}}$ and $\hat{h}$, we need $\boldsymbol{\lambda}^A$ and ζ, which in turn require $\hat{\boldsymbol{\lambda}}$ and $\hat{h}$. Thus the Euler-Lagrange equations comprise a two-point boundary value problem in the smoothing time interval $[0, T]$. Representers decouple the Euler-Lagrange equations into M initial-value and final-value problems. The representer method used to solve for $\hat{\boldsymbol{\lambda}}$, and $\hat{h}$, is described in detail in [Bennett, (1992)], [Chua et al., (1999)]. An indirect approach avoids calculating most of the representers [Egbert et al., (1994)], [Amodei, (1995)], but it is not needed here, as M is small. Results will be shown in the next section.

4 Experiments

4.1 Discrete inverse with open boundaries

In this section we will fit the Lagrangian model (24)-(30) to simulated data (31)-(32). First consider that in order to do this, we minimize the discrete form of the cost functional (33).

Define the time steps and spatial points, as in (8), by

$$t_k = k\triangle t, \quad k = 0, ..., NK \tag{46}$$

$$\alpha_i = -55^\circ + i\triangle\alpha, \quad i = 1, ..., NI \tag{47}$$

$$\beta_j = 35^\circ + j\triangle\beta, \quad j = 1, ..., NJ. \tag{48}$$

Then for $\lambda_{ijk} = \lambda(\alpha_i, \beta_j, t_k)$, with θ_{ijk} and h_{ijk} defined similarly, the discrete form of (33) is

$$J[\boldsymbol{\lambda}] = \sum_{k=2}^{NK}\left(W_{f^\lambda}\sum_{i=2}^{NI-1}\sum_{j=1}^{NJ}(f^\lambda_{ijk})^2 + W_{f^\theta}\sum_{i=1}^{NI}\sum_{j=2}^{NJ-1}(f^\theta_{ijk})^2\right)\triangle\alpha\triangle\beta\triangle t \tag{49}$$

$$+\sum_{k=1}^{NK}\sum_{i=2}^{NI-1}\sum_{j=2}^{NJ-1}2\gamma_{ijk}(h_{ijk} - \mathbf{l}_{ijk}\cdot\boldsymbol{\lambda}_{ijk} + (g_2)_{ijk})\triangle\alpha\triangle\beta\triangle t \tag{50}$$

$$+\left(W_{i^{\lambda_t}}\sum_{i=2}^{NI-1}\sum_{j=1}^{NJ}(i^{\lambda_t})^2 + W_{i^{\theta_t}}\sum_{i=1}^{NI}\sum_{j=2}^{NJ-1}(i^{\theta_t})^2\right)\triangle\alpha\triangle\beta \tag{51}$$

$$+\sum_{k=1}^{NK}\left(\sum_{j=1}^{NJ}[W_{b^{\lambda w}}(b^{\lambda_w}_{jk})^2 + W_{b^{\lambda_e}}(b^{\lambda_e}_{jk})^2]\triangle\beta + \sum_{i=1}^{NI}[W_{b^{\theta_s}}(b^{\theta_s}_{ik})^2 + W_{b^{\theta_n}}(b^{\theta_n}_{ik})^2]\triangle\alpha\right)\triangle t \tag{52}$$

$$+\sum_{k=1}^{NK}\left(\sum_{j=2}^{NJ-1}[W_{b^{h_w}}(b^{h_w}_{jk})^2 + W_{b^{h_e}}(b^{h_e}_{jk})^2]\triangle\beta + \sum_{i=1}^{NI}[W_{b^{h_s}}(b^{h_s}_{ik})^2 + W_{b^{h_n}}(b^{\theta_n}_{ik})^2]\triangle\alpha\right)\triangle t \tag{53}$$

$$+\sum_{m=1}^{M}\omega^\lambda(\epsilon^\lambda_m)^2 + \omega^\theta(\epsilon^\theta_m)^2 + \omega^h(\epsilon^h_m)^2. \tag{54}$$

Note here that the terms corresponding to λ and θ are written out explicitly and have different indices in the summations, as does h. This is because open boundary conditions are applied at $t = \triangle t, \ldots, NK\triangle t$.

We digress for a moment from the current problem to make a statement about data assimilation in a region. In the forward model, the boundary conditions applied at the first time step should be within $O(\triangle t)$ of the initial conditions at the boundary. If not, there will be a

discontinuity at the boundary, and spurious reflection of waves will occur. In the inverse model, the errors at the boundary should also be continuous initially. This can be done by appending the penalty functional, as follows.

For example, at the western boundary, the numerics for the forward model are continuous initially if

$$\lambda(\alpha_1, \beta_j, t_1) - \lambda(\alpha_1, \beta_j, t_0) = \mathrm{O}(\triangle t), \tag{55}$$

where $\lambda(\alpha_1, \beta_j, t_1)$, $\lambda(\alpha_1, \beta_j, t_0)$ are given by the boundary condition and initial condition respectively. The numerics for the inverse model are continuous initially if

$$[\lambda(\alpha_1, \beta_j, t_1) - \lambda_w^B(\beta_j, t_1)] - [\lambda(\alpha_1, \beta_j, t_0) - \alpha_1] = \mathrm{O}(\triangle t), \tag{56}$$

and in addition

$$b^{\lambda_w}(\beta_j, t_1) = \mathrm{O}(\triangle t). \tag{57}$$

(Note that we have assumed no initial error in float position)

In the forward model, we choose initial conditions and boundary conditions such that (56) holds. For the inverse problem, we must also append the penalty functional with

$$\left(\frac{b^{\lambda_w}(\beta_j, t_1)}{\triangle t}\right)^2 \tag{58}$$

to ensure that (57) holds. In this example, (58) already appears in the penalty functional (52), but if there were errors in the initial condition, we would need to add an extra term.

4.2 Prior dynamical errors and weights

The weights on the errors need to be prescribed a priori. The weights not only influence how well the model fits the data, but also the amount by which the model is in error and the data are in error. In this work, we are using constant, uniform weights and show that the inviscid model can fit the data during the short smoothing interval of a few hours. In the future, we will use real data and more sophisticated weights related to error covariances, in which case the reduced penalty functional will be used as a significance test of the prior statistics for the errors [Bennett, (1992)].

The Euler-Lagrange equations (34)-(45) actually require the inverse of the weights, or the hypothetical covariances for the various errors [Bennett, (1992)]. Given the values of ω and u in Section 2.3, and r the radius of the earth, the Lagrangian form (11)-(13) has velocities in radians/sec

$$\frac{\partial \lambda}{\partial t} \sim \frac{u}{r} \sim \frac{2\epsilon c}{r} \sim \frac{4 \times 10^{-2}}{6 \times 10^{6}} \sim 3 \times 10^{-9}, \tag{59}$$

and accelerations in radians/sec^2

$$\frac{\partial^2 \lambda}{\partial t^2} \sim \frac{\omega u}{r} \sim \frac{f u}{r} \sim 1 \times 10^{-4} \times \frac{4 \times 10^{-2}}{6 \times 10^{6}} \sim 7 \times 10^{-13}. \tag{60}$$

Twin experiments are considered, and we arbitrarily choose the inverse weight for the dynamics to be either 25% or 10% of the accelerations (60). In both experiments, the standard deviation of the initial conditions were chosen to be 10% of the velocities (59).

The width (or length) of the domain is approximately 0.4 radians (about 27° of longitude or latitude). Thus we choose the standard deviation of λ and θ at the boundaries to be 10% of

0.4 radians. All of the corresponding weights are given in Table 1.

There are several internal checks for a numerical algorithm for representer calculations. First, the so-called 'representer matrix' should be symmetric, save for roundoff error. Second, the results of two methods for calculating the posterior data residuals or misfits should also agree, save for roundoff error [Chua et al., (1999)]. These tests enable exhaustive checking of the adjoint equations arising from the discrete penalty function (49)-(54). These tests give no indication of the truncation error of the numerics, nor of the validity of the choice of weights. Suffice it to say that, after considerable effort, our code passed the tests so we were confident at least of minimizing $J[\boldsymbol{\lambda}]$ defined by (49)-(54).

4.3 Simulated data and data errors

Simulated data are taken from one float over a period of a few hours. The float's longitude, latitude or equivalent depth is sampled at six times, thus $M = 6$. We choose the values of $\boldsymbol{d}_m^{\lambda}$ and d_m^h from (31)-(32) to be 98% of $\boldsymbol{\lambda}$ or h found from the solution of the nonlinear problem. In the twin experiments, the standard deviations of the simulated data are chosen to be either 1% or 30% of the width of the domain.

4.4 Twin experiment results

Figures 8-9 are time series of the location and depth of one float. The background, or first guess, is the solution of the nonlinear forward problem with initial conditions and boundary conditions described in Section 2.3. The initial longitude of the float given by the background solution is $-50.45°$. The data gives the longitude of the float as $-49.45°$ after 33 minutes. In Figure 8, the

model is able to adjust 111 km in 33 minutes to fit the first data point, and it continues to fit all the data exactly. As the inversion is iterated, the fit to the data becomes more nonlinear. Similar results are found when fitting the latitude and depth of the isopycnal.

In Figure 9 the specified errors in the data are increased from 1% to 30% and the specified errors in the dynamics are decreased from 25% to 10%. Recall that we are only adjusting the errors in the dynamics for λ, θ, since the equivalent depth h is assumed to be error free. The change in the error for the data does not effect the inversion of the depth of this float. However, now the longitude and latitude do not fit all of the data, as might be expected.

These short-range inversions do little more than verify the logic of the algorithm and code. It will be essential to include friction in order to sustain even forward integrations of tens of days or more, on North Atlantic mesoscales.

5 Conclusions

We have introduced variational data assimilation of Lagrangian data into an open ocean model expressed in Lagrangian form. Our first demonstrations involved inviscid dynamics, on scales of North Atlantic mesoscale variability. With high spatial resolution, and after one day, the solution of the reduced gravity shallow water equations in an open domain is virtually the same whether calculated using the Lagrangian or Eulerian form. Functional iteration without data does recover the forward solution of the nonlinear dynamics, that is, iterations on the tangent linear model converge to the nonlinear solution. In addition, representer solutions can be consistently constructed from the Euler-Lagrange variational equations for the tangent

linearized Lagrangian dynamics in an open domain.

It remains to introduce viscous stresses into the Lagrangian dynamics, by transforming the Eulerian viscous terms into Lagrangian coordinates, in order to enable comparisons with solutions of the Eulerian viscous dynamics, and to introduce real float data. Lagrangian primitive equation dynamics will be a further challenge.

Acknowledgments

This work is supported by ONR N00014-99-1-0040. The COAS CM-5 is supported by NASA EOS, and we are grateful to Mark Abbott for access to it. The COAS CM-500e systems were donated by the Office of Naval Research.

Appendix A

The Lagrangian reduced gravity model, linearized about a previous iterate in Section 2.3, can be written in the following manner: let the vector of unknowns be denoted

$$\boldsymbol{\tau} = \left[\begin{array}{cccccccccccc} \theta & \frac{\partial\lambda}{\partial t} & \frac{\partial\theta}{\partial t} & h & \frac{\partial\lambda}{\partial\alpha} & \frac{\partial\lambda}{\partial\beta} & \frac{\partial h}{\partial\alpha} & \frac{\partial h}{\partial\beta} & \frac{\partial\theta}{\partial\alpha} & \frac{\partial\theta}{\partial\beta} & 1 \end{array} \right]^T, \tag{A-1}$$

then the linear form of (11)-(13) at the nth iteration is

$$\frac{\partial^2\lambda^n}{\partial t^2} = \mathbf{k}\cdot\boldsymbol{\tau}^n \tag{A-2}$$

$$\frac{\partial^2\theta^n}{\partial t^2} = \mathbf{l}\cdot\boldsymbol{\tau}^n \tag{A-3}$$

$$h^n = \mathbf{m}\cdot\boldsymbol{\tau}^n, \tag{A-4}$$

where

$$\boldsymbol{k} = [\ k_1 \quad k_2 \quad k_3 \quad k_4 \quad 0 \quad 0 \quad k_5 \quad k_6 \quad k_7 \quad k_8 \quad k_9\ ]^T \tag{A-5}$$

$$\boldsymbol{l} = [\ l_1 \quad l_2 \quad 0 \quad l_3 \quad l_4 \quad l_5 \quad l_6 \quad l_7 \quad 0 \quad 0 \quad l_8\ ]^T \tag{A-6}$$

$$\boldsymbol{m} = [\ m_1 \quad 0 \quad 0 \quad 0 \quad m_2 \quad m_3 \quad 0 \quad 0 \quad m_4 \quad m_5 \quad m_6\ ]^T. \tag{A-7}$$

Now let

$$h_{\text{init}} = h(\alpha,\beta,0)J(\alpha,\beta,0)\cos\theta(\alpha,\beta,0)$$

and recall

$$\frac{\partial(h^{n-1},\theta^{n-1})}{\partial(\alpha,\beta)} = \frac{\partial h^{n-1}}{\partial\alpha}\frac{\partial\theta^{n-1}}{\partial\beta} - \frac{\partial h^{n-1}}{\partial\beta}\frac{\partial\theta^{n-1}}{\partial\alpha},$$

for example. Then

$$
\begin{aligned}
k_1 &= 2\sec^2\theta^{n-1}\frac{\partial\lambda^{n-1}}{\partial t}\frac{\partial\theta^{n-1}}{\partial t} + 2\Omega\sec^2\theta^{n-1}\frac{\partial\theta^{n-1}}{\partial t} - \frac{g}{r^2h_{\rm int}}h^{n-1}\frac{\tan\theta^{n-1}}{\cos\theta^{n-1}}\frac{\partial(h^{n-1},\theta^{n-1})}{\partial(\alpha,\beta)} \\
k_2 &= 2\tan\theta^{n-1}\frac{\partial\theta^{n-1}}{\partial t} \\
k_3 &= 2\tan\theta^{n-1}\frac{\partial\lambda^{n-1}}{\partial t} + 2\Omega\tan\theta^{n-1} \\
k_4 &= -\frac{g}{r^2h_{\rm int}}\frac{1}{\cos\theta^{n-1}}\frac{\partial(h^{n-1},\theta^{n-1})}{\partial(\alpha,\beta)} \\
k_5 &= -\frac{g}{r^2h_{\rm int}}\frac{h^{n-1}}{\cos\theta^{n-1}}\frac{\partial\theta^{n-1}}{\partial\beta} \\
k_6 &= \frac{g}{r^2h_{\rm int}}\frac{h^{n-1}}{\cos\theta^{n-1}}\frac{\partial\theta^{n-1}}{\partial\alpha} \\
k_7 &= \frac{g}{r^2h_{\rm int}}\frac{h^{n-1}}{\cos\theta^{n-1}}\frac{\partial h^{n-1}}{\partial\beta} \\
k_8 &= -\frac{g}{r^2h_{\rm int}}\frac{h^{n-1}}{\cos\theta^{n-1}}\frac{\partial h^{n-1}}{\partial\alpha} \\
k_9 &= -2\frac{\partial\lambda^{n-1}}{\partial t}\frac{\partial\theta^{n-1}}{\partial t}(\theta^{n-1}\sec^2\theta^{n-1} + \tan\theta^{n-1}) - 2\Omega\frac{\partial\theta^{n-1}}{\partial t}\theta^{n-1}\sec^2\theta^{n-1} \\
&\quad + \frac{g}{r^2h_{\rm int}}\frac{h^{n-1}}{\cos\theta^{n-1}}\frac{\partial(h^{n-1},\theta^{n-1})}{\partial(\alpha,\beta)}[2 + \theta^{n-1}\tan\theta^{n-1}],
\end{aligned}
$$

$$
\begin{aligned}
l_1 &= -\frac{\partial \lambda^{n-1}}{\partial t}(\cos^2\theta^{n-1} - \sin^2\theta^{n-1})(\frac{\partial \lambda^{n-1}}{\partial t} + 2\Omega) + \frac{g}{r^2 h_{\rm int}} h^{n-1}\sin\theta^{n-1}\frac{\partial(\lambda^{n-1}, h^{n-1})}{\partial(\alpha,\beta)} \\
l_2 &= -\cos\theta^{n-1}\sin\theta^{n-1}(2\Omega + 2\frac{\partial \lambda^{n-1}}{\partial t}) \\
l_3 &= -\frac{g}{r^2 h_{\rm int}}\cos\theta^{n-1}\frac{\partial(\lambda^{n-1}, h^{n-1})}{\partial(\alpha,\beta)} \\
l_4 &= -\frac{g}{r^2 h_{\rm int}} h^{n-1}\cos\theta^{n-1}\frac{\partial h^{n-1}}{\partial \beta} \\
l_5 &= \frac{g}{r^2 h_{\rm int}} h^{n-1}\cos\theta^{n-1}\frac{\partial h^{n-1}}{\partial \alpha} \\
l_6 &= \frac{g}{r^2 h_{\rm int}} h^{n-1}\cos\theta^{n-1}\frac{\partial \lambda^{n-1}}{\partial \beta} \\
l_7 &= -\frac{g}{r^2 h_{\rm int}} h^{n-1}\cos\theta^{n-1}\frac{\partial \lambda^{n-1}}{\partial \alpha} \\
l_8 &= \theta^{n-1}\frac{\partial \lambda^{n-1}}{\partial t}(\cos^2\theta^{n-1} - \sin^2\theta^{n-1})(2\Omega + \frac{\partial \lambda^{n-1}}{\partial t}) + \left(\frac{\partial \lambda^{n-1}}{\partial t}\right)^2 \cos\theta^{n-1}\sin\theta^{n-1} \\
&\quad -\frac{g}{r^2 h_{\rm int}} h^{n-1}\frac{\partial(\lambda^{n-1}, h^{n-1})}{\partial(\alpha,\beta)}[\theta^{n-1}\sin\theta^{n-1} - 2\cos\theta^{n-1}],
\end{aligned}
$$

and

$$
\begin{aligned}
m_1 &= \frac{h_{\rm int}}{\cos\theta^{n-1} J^{n-1}}\tan\theta^{n-1} \\
m_2 &= -\frac{h_{\rm int}}{\cos\theta^{n-1}(J^{n-1})^2}\frac{\partial \theta^{n-1}}{\partial \beta} \\
m_3 &= \frac{h_{\rm int}}{\cos\theta^{n-1}(J^{n-1})^2}\frac{\partial \theta^{n-1}}{\partial \alpha} \\
m_4 &= \frac{h_{\rm int}}{\cos\theta^{n-1}(J^{n-1})^2}\frac{\partial \lambda^{n-1}}{\partial \beta} \\
m_5 &= -\frac{h_{\rm int}}{\cos\theta^{n-1}(J^{n-1})^2}\frac{\partial \lambda^{n-1}}{\partial \beta} \\
m_6 &= -\frac{h_{\rm int}}{\cos\theta^{n-1} J^{n-1}}[\theta^{n-1}\tan\theta^{n-1} - 3].
\end{aligned}
$$

The explicit expressions in (19) are

$$
\begin{aligned}
\mathsf{L}(1,1) &= k_2\frac{\partial}{\partial t} + k_4(m_2\frac{\partial}{\partial \alpha} + m_3\frac{\partial}{\partial \beta}) + k_5(m_2\frac{\partial^2}{\partial \alpha^2} + m_3\frac{\partial^2}{\partial \alpha\beta}) + k_6(m_2\frac{\partial^2}{\partial \alpha\beta} + m_3\frac{\partial^2}{\partial \beta^2}) \\
\mathsf{L}(1,2) &= k_1 + k_3\frac{\partial}{\partial t} + k_4(m_1 + m_4\frac{\partial}{\partial \alpha} + m_5\frac{\partial}{\partial \beta}) + k_5(m_1\frac{\partial}{\partial \alpha} + m_4\frac{\partial^2}{\partial \alpha^2} + m_5\frac{\partial^2}{\partial \alpha\beta}) \\
&\quad + k_6(m_1\frac{\partial}{\partial \beta} + m_4\frac{\partial^2}{\partial \alpha\beta} + m_5\frac{\partial^2}{\partial \beta^2}) + k_7\frac{\partial}{\partial \alpha} + k_8\frac{\partial}{\partial \beta} \\
\mathsf{L}(2,1) &= l_2\frac{\partial}{\partial t} + l_3(m_2\frac{\partial}{\partial \alpha} + m_3\frac{\partial}{\partial \beta}) + l_4\frac{\partial}{\partial \alpha} + l_5\frac{\partial}{\partial \beta} + l_6(m_2\frac{\partial^2}{\partial \alpha^2} + m_3\frac{\partial^2}{\partial \alpha\beta}) \\
&\quad + l_7(m_2\frac{\partial^2}{\partial \alpha\beta} + m_3\frac{\partial^2}{\partial \beta^2}) \\
\mathsf{L}(2,2) &= l_1 + l_3(m_1 + m_4\frac{\partial}{\partial \alpha} + m_5\frac{\partial}{\partial \beta}) + l_6(m_1\frac{\partial}{\partial \alpha} + m_4\frac{\partial^2}{\partial \alpha^2} + m_5\frac{\partial^2}{\partial \alpha\beta}) \\
&\quad + l_7(m_1\frac{\partial}{\partial \beta} + m_4\frac{\partial^2}{\partial \alpha\beta} + m_5\frac{\partial^2}{\partial \beta^2}) \\
g_1(1) &= k_9 + k_4 m_6 \\
g_1(2) &= l_8 + m_6 l_3,
\end{aligned}
$$

and in (20) are

$$
\begin{aligned}
l(1) &= m_2\frac{\partial}{\partial \alpha} + m_3\frac{\partial}{\partial \beta} \\
l(2) &= m_1 + m_4\frac{\partial}{\partial \alpha} + m_5\frac{\partial}{\partial \beta} \\
g_2 &= m_6.
\end{aligned}
$$

Appendix B

Here we will give the inverse formulation (34)-(45) from Section 3.3, in detail. Definitions of $\boldsymbol{\tau}$, $\boldsymbol{k}$, $\boldsymbol{l}$, and $\boldsymbol{m}$ in the following equations are given in Appendix A. The adjoint equations are

$$\begin{aligned}
\frac{\partial^2 \lambda^A}{\partial t^2} &= -k_2 \frac{\partial \lambda^A}{\partial t} - l_2 \frac{\partial \theta^A}{\partial t} - l_4 \frac{\partial \theta^A}{\partial \alpha} - l_5 \frac{\partial \theta^A}{\partial \beta} - m_2 \frac{\partial \zeta}{\partial \alpha} - m_3 \frac{\partial \zeta}{\partial \beta} \qquad \text{(B-1)} \\
&\quad - \sum_{m=1}^{M} \omega^{\lambda} (d_m^{\lambda} - \hat{\lambda}(\boldsymbol{\alpha}_m, t_m)) \delta(\boldsymbol{\alpha} - \boldsymbol{\alpha}_m) \delta(t - t_m) \\
\frac{\partial^2 \theta^A}{\partial t^2} &= k_1 \lambda^A - k_3 \frac{\partial \lambda^A}{\partial t} - k_7 \frac{\partial \lambda^A}{\partial \alpha} - k_8 \frac{\partial \lambda^A}{\partial \beta} + l_1 \theta^A + m_1 \zeta - m_4 \frac{\partial \zeta}{\partial \alpha} \qquad \text{(B-2)} \\
&\quad - m_5 \frac{\partial \zeta}{\partial \beta} \sum_{m=1}^{M} \omega^{\theta} (d_m^{\theta} - \hat{\theta}(\boldsymbol{\alpha}_m, t_m)) \delta(\boldsymbol{\alpha} - \boldsymbol{\alpha}_m) \delta(t - t_m) \\
\zeta &= k_4 \lambda^A - k_5 \frac{\partial \lambda^A}{\partial \alpha} - k_6 \frac{\partial \lambda^A}{\partial \beta} + l_3 \theta^A - l_6 \frac{\partial \theta^A}{\partial \alpha} - l_7 \frac{\partial \theta^A}{\partial \beta} \qquad \text{(B-3)} \\
&\quad - \sum_{m=1}^{M} \omega^{h} (d_m^{h} - \hat{h}(\boldsymbol{\alpha}_m, t_m)) \delta(\boldsymbol{\alpha} - \boldsymbol{\alpha}_m) \delta(t - t_m),
\end{aligned}$$

where $\hat{\lambda}$, $\hat{\theta}$, and $\hat{h}$ satisfy

$$\begin{aligned}
\frac{\partial^2 \hat{\lambda}}{\partial t^2} &= \boldsymbol{k} \cdot \hat{\boldsymbol{\tau}} + W_{f^{\lambda}}^{-1} \lambda^A \qquad \text{(B-4)} \\
\frac{\partial^2 \hat{\theta}}{\partial t^2} &= \boldsymbol{l} \cdot \hat{\boldsymbol{\tau}} + W_{f^{\theta}}^{-1} \theta^A \qquad \text{(B-5)} \\
\hat{h} &= \mathbf{m} \cdot \hat{\boldsymbol{\tau}}, \qquad \text{(B-6)}
\end{aligned}$$

with initial conditions

$$\hat{\lambda}(\alpha,\beta,0) = \alpha \tag{B-7}$$

$$\hat{\theta}(\alpha,\beta,0) = \beta \tag{B-8}$$

$$\hat{\lambda}_t(\alpha,\beta,0) = u^I + W_{I^\lambda}^{-1}\lambda^A(\alpha,\beta,0) \tag{B-9}$$

$$\hat{\theta}_t(\alpha,\beta,0) = v^I + W_{I^\theta}^{-1}\theta^A(\alpha,\beta,0) \tag{B-10}$$

$$\hat{h}^n = h^I, \tag{B-11}$$

and boundary conditions

$$\hat{\lambda}(\alpha_e,\beta,t) = \lambda_e^B(\beta,t) + W_{b^{\lambda_e}}^{-1}[l_4\theta^A(\alpha_e,\beta,t) + m_2\zeta(\alpha_e,\beta,t)] \tag{B-12}$$

$$\hat{\lambda}(\alpha_w,\beta,t) = \lambda_w^B(\beta,t) - W_{b^{\lambda_w}}^{-1}[l_4\theta^A(\alpha_w,\beta,t) + m_2\zeta(\alpha_w,\beta,t)] \tag{B-13}$$

$$\hat{\theta}(\alpha,\beta_n,t) = \theta_n^B(\alpha,t) + W_{b^{\theta_n}}^{-1}[k_8\lambda^A(\alpha,\beta_n,t) + m_5\zeta(\alpha,\beta_n,t)] \tag{B-14}$$

$$\hat{\theta}(\alpha,\beta_s,t) = \theta_s^B(\alpha,t) - W_{b^{\theta_s}}^{-1}[k_8\lambda^A(\alpha,\beta_s,t) + m_5\zeta(\alpha,\beta_s,t)] \tag{B-15}$$

$$\hat{h}(\alpha,\beta_n,t) = h_n^B(\alpha,t) + W_{b^{h_n}}^{-1}[k_6\lambda^A(\alpha,\beta_n,t) + l_7\theta^A(\alpha,\beta_n,t)] \tag{B-16}$$

$$\hat{h}(\alpha,\beta_s,t) = h_s^B(\alpha,t) - W_{b^{h_s}}^{-1}[k_6\lambda^A(\alpha,\beta_s,t) + l_7\theta^A(\alpha,\beta_s,t)] \tag{B-17}$$

$$\hat{h}(\alpha_e,\beta,t) = h_e^B(\beta,t) + W_{b^{h_e}}^{-1}[k_5\lambda^A(\alpha_e,\beta,t) + l_6\theta^A(\alpha_e,\beta,t)] \tag{B-18}$$

$$\hat{h}(\alpha_w,\beta,t) = h_w^B(\beta,t) - W_{b^{h_w}}^{-1}[k_5\lambda^A(\alpha_w,\beta,t) + l_6\theta^A(\alpha_w,\beta,t)]. \tag{B-19}$$

where the subscripts n, s, e, and w denote the north south east and west directions respectively.

Appendix C

LIST OF SYMBOLS

b^{h_w}, b^{h_e}, b^{h_s}, b^{h_n}	boundary error in h at West, East, South, and North
b^{λ_w}, b^{λ_e}, b^{θ_s}, b^{θ_n}	boundary error in λ at West and East, and in θ at South and North
$\boldsymbol{b}^h$	$[b^{h_w}, b^{h_e}, b^{h_s}, b^{h_n}]$
$\boldsymbol{b}^\lambda$	$[b^{\lambda_w}, b^{\lambda_e}, b^{\theta_s}, b^{\theta_n}]$
c	phase speed, 2 m/s
d_m^λ, d_m^θ, d_m^h	data for longitude, latitude, and the equivalent depth, $m = 1, \ldots, M$
$\boldsymbol{d}_m^\lambda$	$[d_m^\lambda, d_m^\theta]$
f	Coriolis parameter $2\Omega \sin\theta$
f^λ, f^θ	error in dynamics for λ, θ
$\boldsymbol{f}^\lambda$	$[f^\lambda, f^\theta]$
g	mean gravitational acceleration, 9.7976 m/s^2
$\boldsymbol{g}_1$, g_2, $\boldsymbol{l}$, $\mathbf{L}$	terms in the linearization of the Lagrangian dynamics
h, h^I, h^B	equivalent depth, the initial value, and boundary value
H, $\hat{H}$	mean depth, and ϵH
i^{λ_t}, i^{θ_t}	error in initial meridional and zonal velocities
$\boldsymbol{i}$	$[i^{\lambda_t}, i^{\theta_t}]$
J	jacobian for the transformation from Eulerian to Lagrangian coordintes
$J[\boldsymbol{\lambda}]$	cost functional
k, l	longitudinal and latitudinal wavenumbers
L^A, l^A	adjoint terms in Euler-Lagrange equations
M	number of times data is taken from each float
$\boldsymbol{n}_r$	unit normal vector in North, South, East, West directions; $r = (n, s, e, w)$
$\mathbf{p}$, $\mathbf{q}$	boundary terms in the adjoint equations
r	earth's radius, 6370.949 km
u, v, u^I, v^I	meridional and zonal velocities, and their initial values
W_{f^λ}, W_{f^θ}, $W_{I^{\lambda_t}}$, $W_{I^{\theta_t}}$, $W_{b^{\lambda_w}}$, $W_{b^{\lambda_e}}$, $W_{b^{\theta_s}}$, $W_{b^{\theta_n}}$, $W_{b^{h_w}}$, $W_{b^{h_e}}$, $W_{b^{h_s}}$, $W_{b^{h_n}}$	weights on the errors in the dynamics, initial velocities, and boundary values for the location, and equivalent depth
$\boldsymbol{W}_{f^\lambda}$, $\boldsymbol{W}_I$, $\boldsymbol{W}_b$, $\boldsymbol{W}_h$	$[W_{f^\lambda}, W_{f^\theta}]$, $[W_{I^{\lambda_t}}, W_{I^{\theta_t}}]$, $[W_{b^{\lambda_w}}, W_{b^{\lambda_e}}, W_{b^{\theta_s}}, W_{b^{\theta_n}}]$, $[W_{b^{h_w}}, W_{b^{h_e}}, W_{b^{h_s}}, W_{b^{h_n}}]$

α, β	initial longitude and latitude in Lagrangian coordinates
$\boldsymbol{\alpha}$	$[\alpha, \beta]$
δ, ϵ, γ, ω	parameters in analytical solution to linear shallow water problem
ϵ^h, ϵ^λ, ϵ^θ	error in data for h, λ, and θ
$\boldsymbol{\epsilon}^\lambda$	$[\epsilon^\lambda, \epsilon^\theta]$
λ, θ, λ^B	longitude, latitude, and boundary values
$\boldsymbol{\lambda}$	$[\lambda, \theta]$
$\boldsymbol{\lambda}^A$, $\hat{\boldsymbol{\lambda}}$,	adjoint variable in Euler-Lagrange equations, and minimizer of cost functional
ω^λ, ω^θ, ω^h	weights on the errors in the data for the longitude, latitude and equivalent depth
$\boldsymbol{\omega}^\lambda$	$[\omega^\lambda, \omega^\theta]$
Ω	angular rotation rate of earth, 7.292115×10^{-5} rad/sec

References

[Amodei, (1995)] Amodei, L.: Solution approcheé pour un problème d'assimilation de donneés meterologiques avec prise en compte de l'erreur de modèlè. *Comptes Rendus de l'Academie des Sciences,* **321**, Seŕie IIa, 1087-1094.

[Arakawa, (1966)] Arakawa, A.: Computational design for long term numerical integration of the equation of fluid motion. Part 1. *J. Comput. Phys.,* **1**, 119,143.

[Aref, (1984)] Aref, H.: Stirring by chaotic advection. *J. Fluid Mech*, **143**, 1-21.

[Anderson et al., (1996)] Anderson-Fontana, S., M. Prater, and H.T. Rossby: RAFOS float data report of the North Atlantic Current study 1993-1995, *Univ. of Rhode Island, G.S.O. Tech. Rept.* 96-4, 242 pp.

[Bennett and Chua, (1999)] Bennett, A.F., and B.S. Chua: Open Boundary Conditions for Lagrangian Geophysical Fluid Dynamics, *J. Comp. Phys.* **153**, 418-436.

[Bennett and Chua, (1994)] Bennett, A.F., and B.S. Chua: Open-Ocean Modeling as an Inverse Problem: The Primitive Equations. *Mon. Wea. Rev.,* Vol. 122, No. 6, 1326-1336.

[Bennett, (1992)] Bennett, A.F.: *Inverse Methods in Physical Oceanography, Monographs on Mechanics and Applied Mathematics.* Cambridge University Press, 346 pp.

[Bennett and Middleton, (1983)] Bennett, A.F., and J.F. Middleton: Statistical mechanics of a finite difference approximation to the barotropic vorticity equation. *Quart. J. R. Met. Soc.,* **109**, pp.795-808.

[Chelton et al., (1998)] Chelton, D.B., R.A. deSzoeke, and M.G. Schlax: Geographical Variability of the First Baroclinic Rossby Radius of Deformation. *J. Phys. Oceanogr.,* Vol. 28, No. 3, 433-460.

[Chua et al., (1999)] Chua, B.S., H.E. Ngodock, and A.F. Bennett: Implementation of a Tropical Ocean Analysis System. To appear *Proc. Third WMO Int. Symposium on Assimilation of Observations in Meterol. and Oceanogr.,* June 7-11, Quebec City, Canada.

[Egbert et al., (1994)] Egbert, G.D., A.F. Bennett, and M.G.G. Foreman: TOPEX/POSEIDON tides estimated using a global inverse method. *J. Geophys. Res.*, **99**, 24, 821-852.

[Gill, (1982)] Gill, A.E.: *Atmosphere - Ocean Dynamics*, Academic Press Inc., 662 pp.

[Ide et al., (1997)] Ide, K., P. Courtier, M. Ghil, and A.C. Lorenc: Unified notation for data assimilation: Operational, sequential and variational. *JM Soc. Jpn.*, **75**, (1B), 181-189.

[Ngodock et al., (1999)] Ngodock, H.E., B.S. Chua, and A.F. Bennett: Generalized Inverse of a Reduced Gravity Primitive Equations Ocean Model and Tropical Atmosphere-Ocean Data. *Mon. Wea. Rev.*, accepted.

[Oliger and Sundström, (1978)] Oliger, J., and A. Sundström: Theoretical and practical aspects of some initial boundary value problems in fluid dynamics. *SIAM J. Appl. Math.,* **35**, 419-446.

[Özgökmen et al., (1999)] Özgökmen, T.M., A. Griffa, L.I. Piterbarg, and A.J. Mariano: On the Predictability of Lagrangian Trajectories in the Ocean. *J. Atmos. Oceanic Tech.,* in press.

[Rossby et al., (1999)] Rossby, T., D. Hebert, and H.-M. Zhang: Observations of Relative Dispersion Along Isopycnals, *31st Int. Liége Colloq. on Ocean Hydro.*, 82, Liége Belgium, May 3-7, pp. 109.

[Samelson, (1996)] Samelson, R.M.: Chaotic transport by mesoscale motions. In *Stochastic Modeling in Physical Oceanography*, 423-438. Editors, R. J. Adler, P. Müller and B. L. Rozovoskii, Birkhäuser, pp. 466.

[Staniforth and Côté, (1991)] Staniforth, A., and J. Côté: Semi-Lagrangian Integration Schemes for Atmospheric Models - A Review. *Mon. Wea. Rev.,* Vol. 119, 2206-2223.

[Yang and Liu, (1996)] Yang, H., and Z. Liu: The three-dimensional chaotic transport and the great ocean barrier. *J. Phys. Oceanogr.*, **27**, 1258-1273.

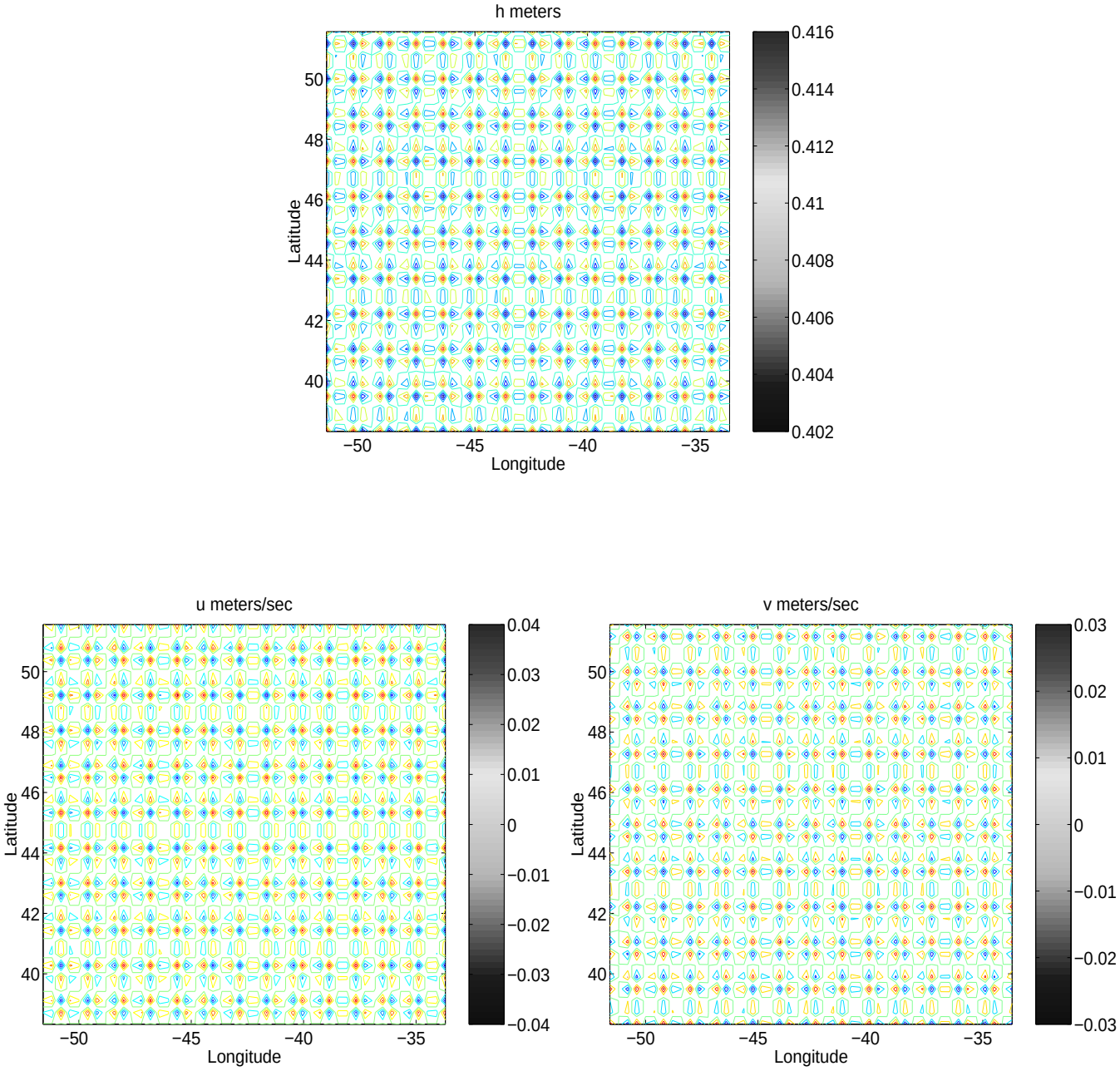

Figure 1: Initial depth, meridional and zonal velocities given by the Sverdrup wave. There are 22 waves in the meridonal direction, and 18 waves in the zonal, which correspond to a deformation radius of 20 km.

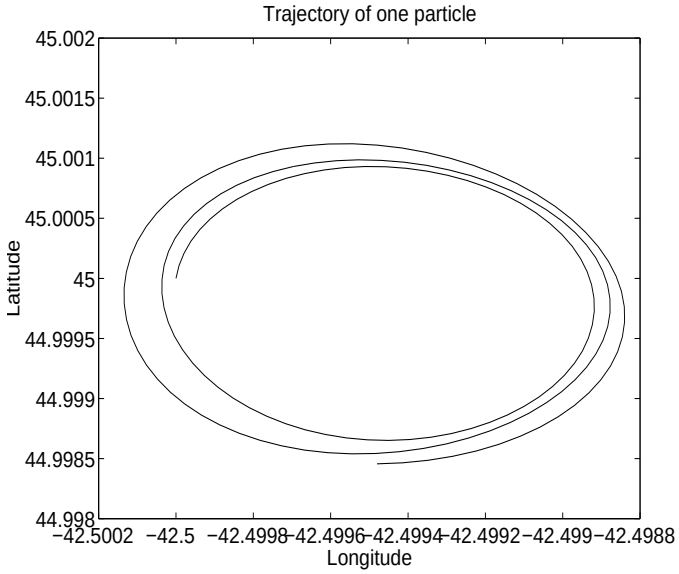

Figure 2: Path of the particle that began at -45° longitude, 42.5° latitude, after one day.

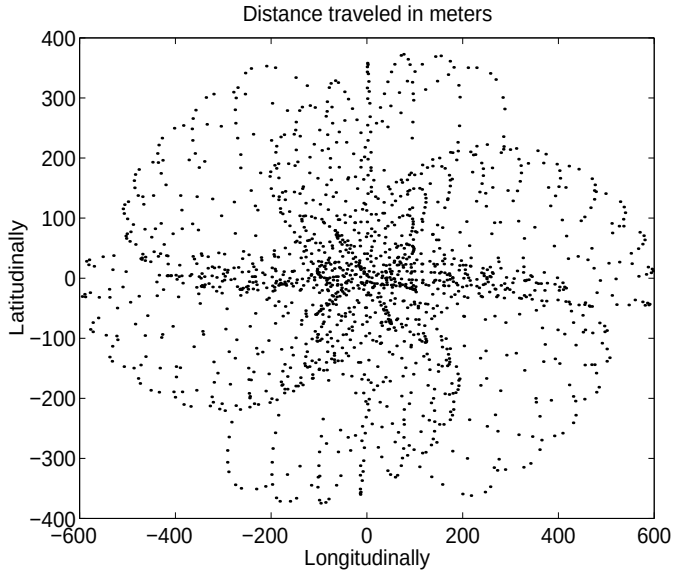

Figure 3: Total distance each particle traveled from its original position, after one day, and 1/7 of the particles are plotted.

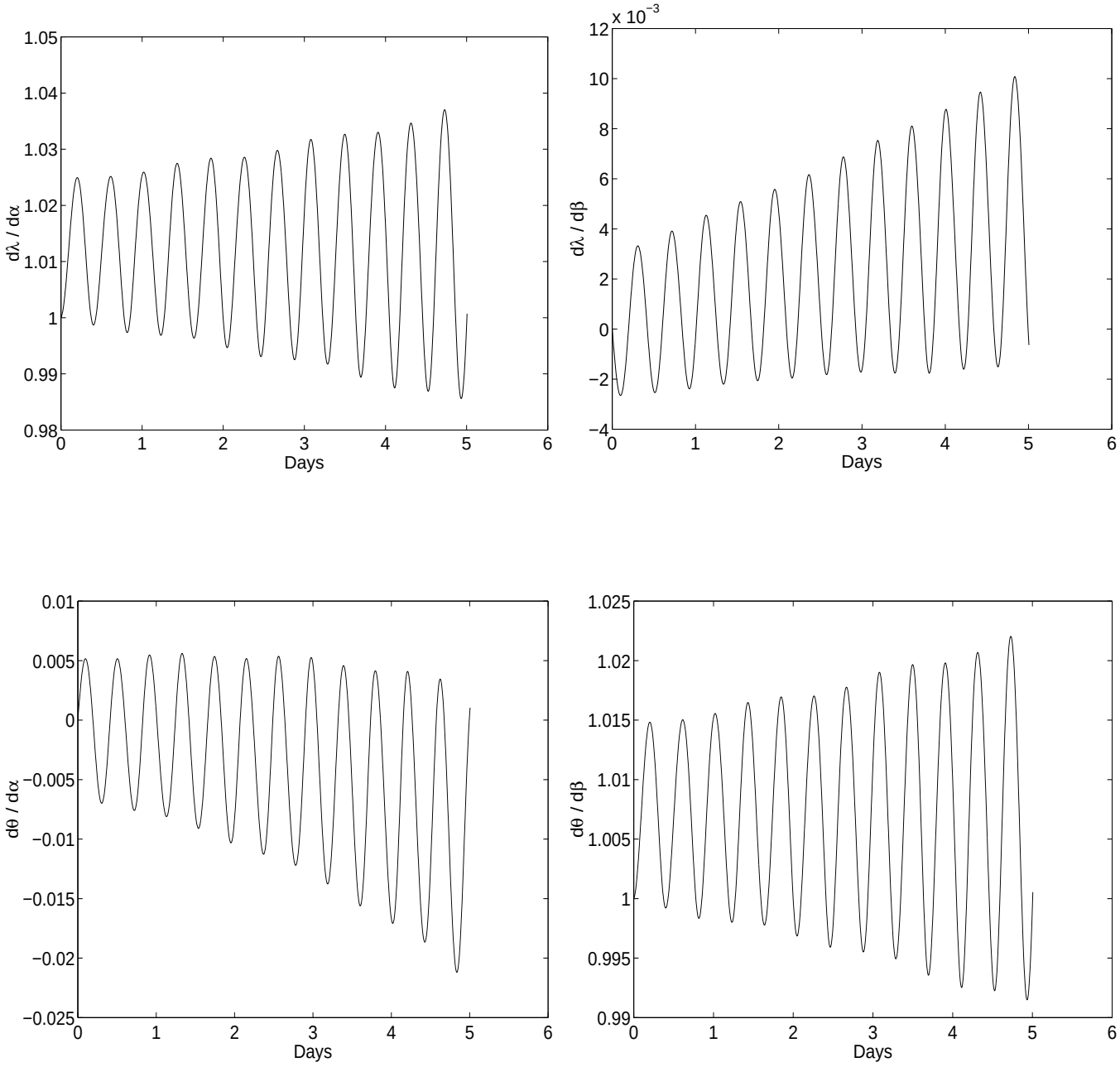

Figure 4: The strains $\frac{\partial\lambda}{\partial\alpha}$, $\frac{\partial\lambda}{\partial\beta}$, $\frac{\partial\theta}{\partial\alpha}$, $\frac{\partial\theta}{\partial\beta}$ clockwise from top left, of the particle with initial position $-42.5°$ Longitude, and $45°$ Latitude. They increase with time which causes computational instability in the Lagrangian form.

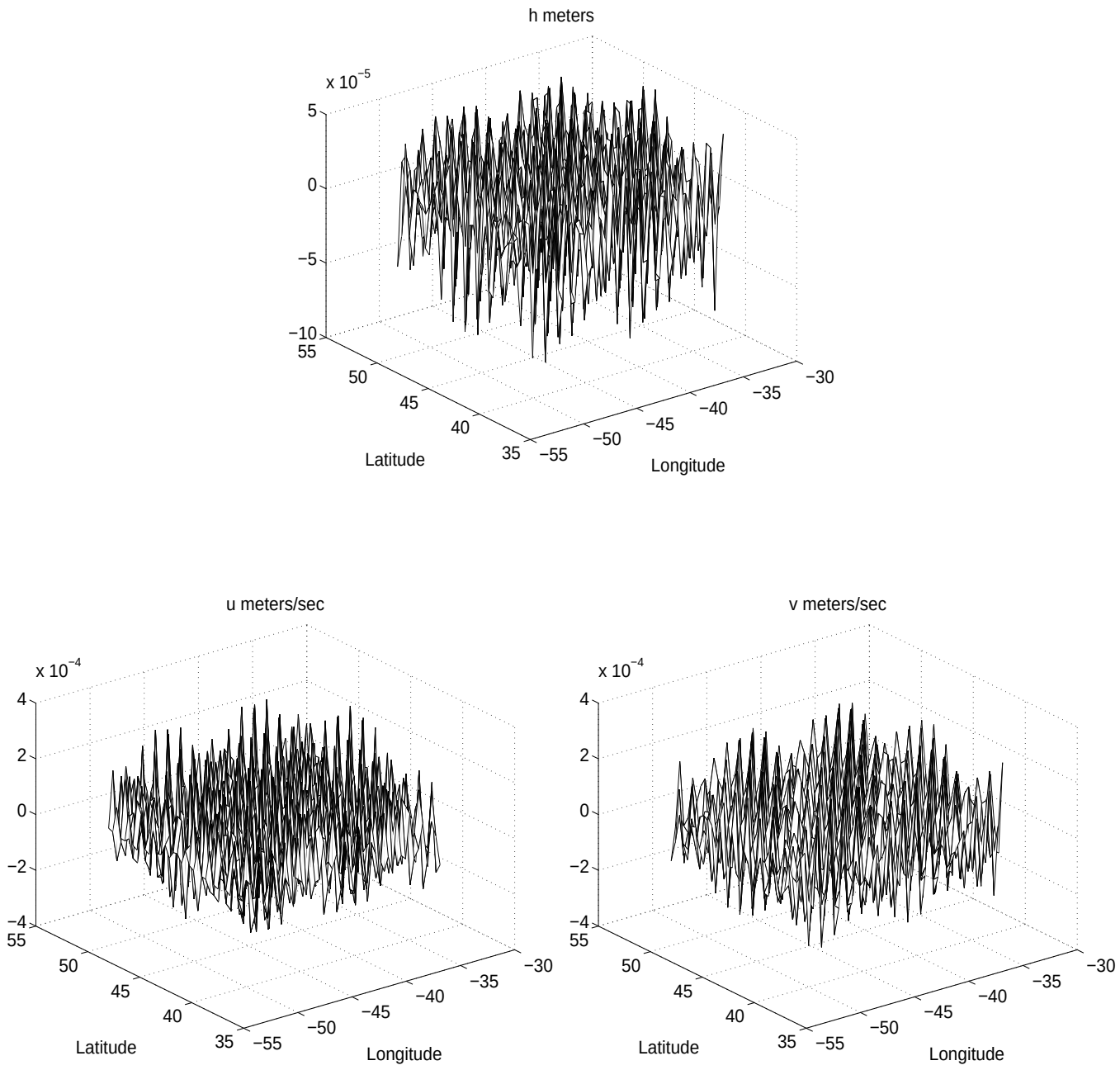

Figure 5: Difference between Eulerian and Lagrangian solution after one day. The Lagrangian solution was interpolated to the Eulerian grid.

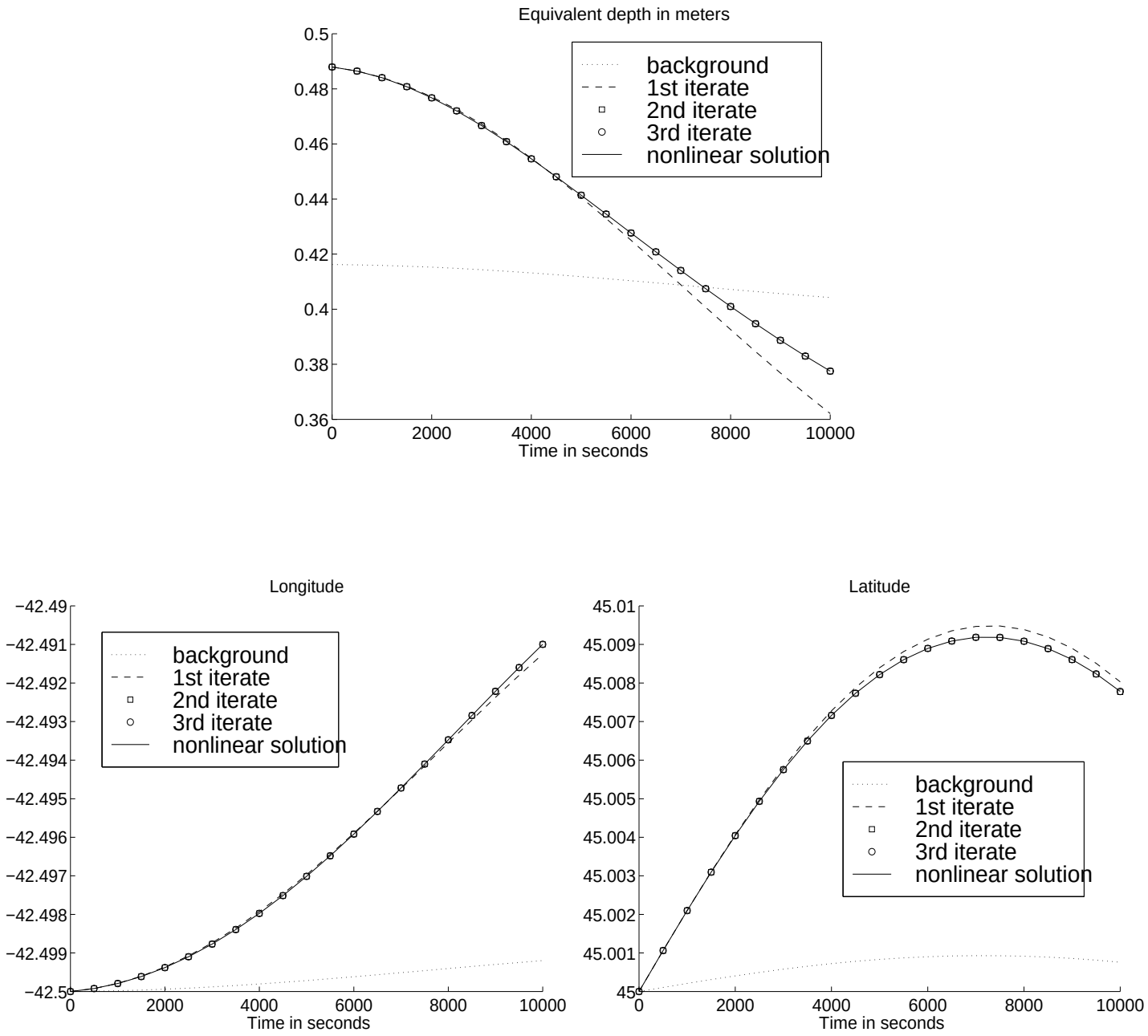

Figure 6: Linear iterates from the Lagrangian shallow water model. The velocities of the background solution are approximately 0.04 m/s, of the nonlinear solution are 0.4 m/s.

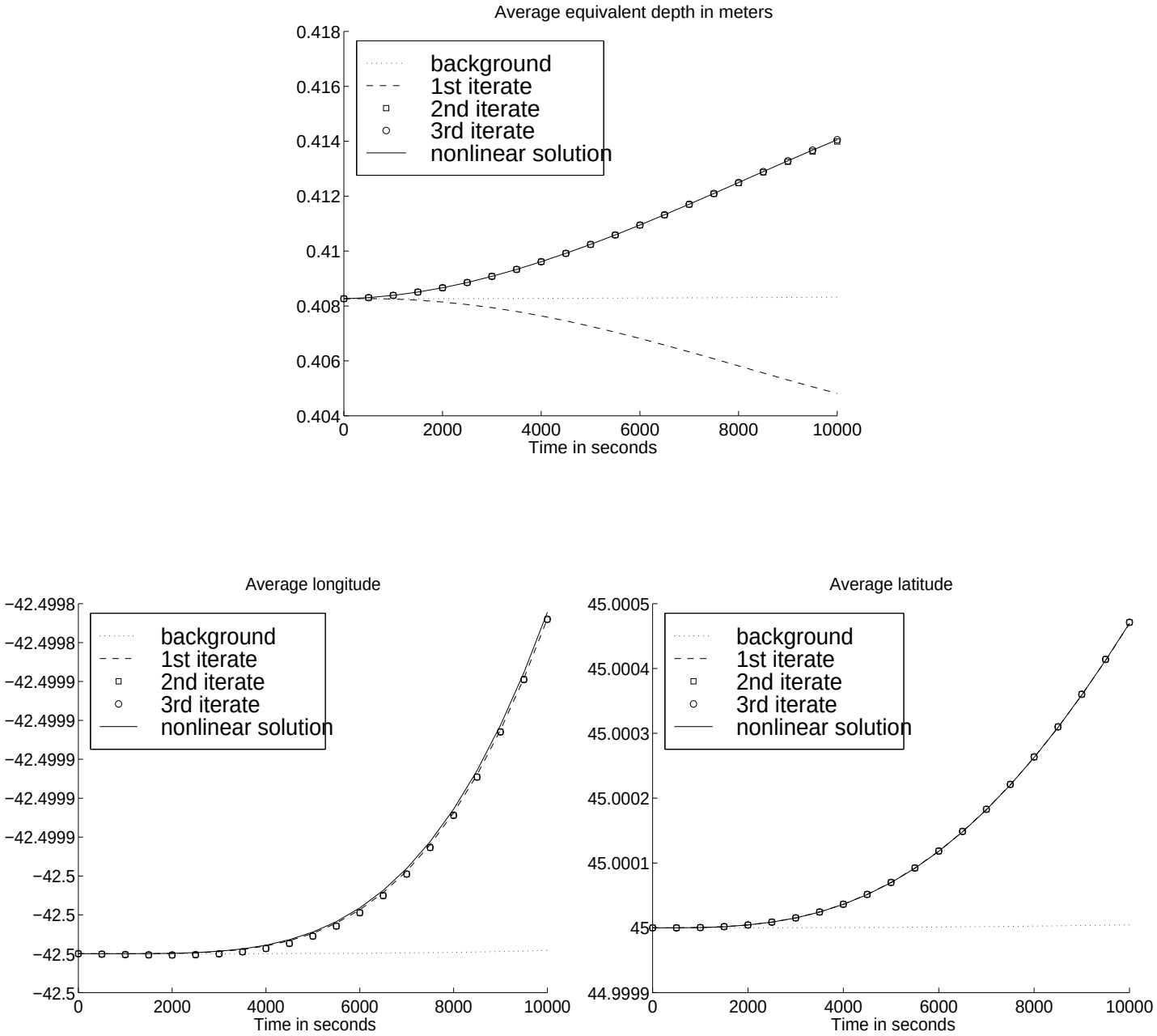

Figure 7: Average over all trajectories in the linear iterates from the Lagrangian shallow water model.

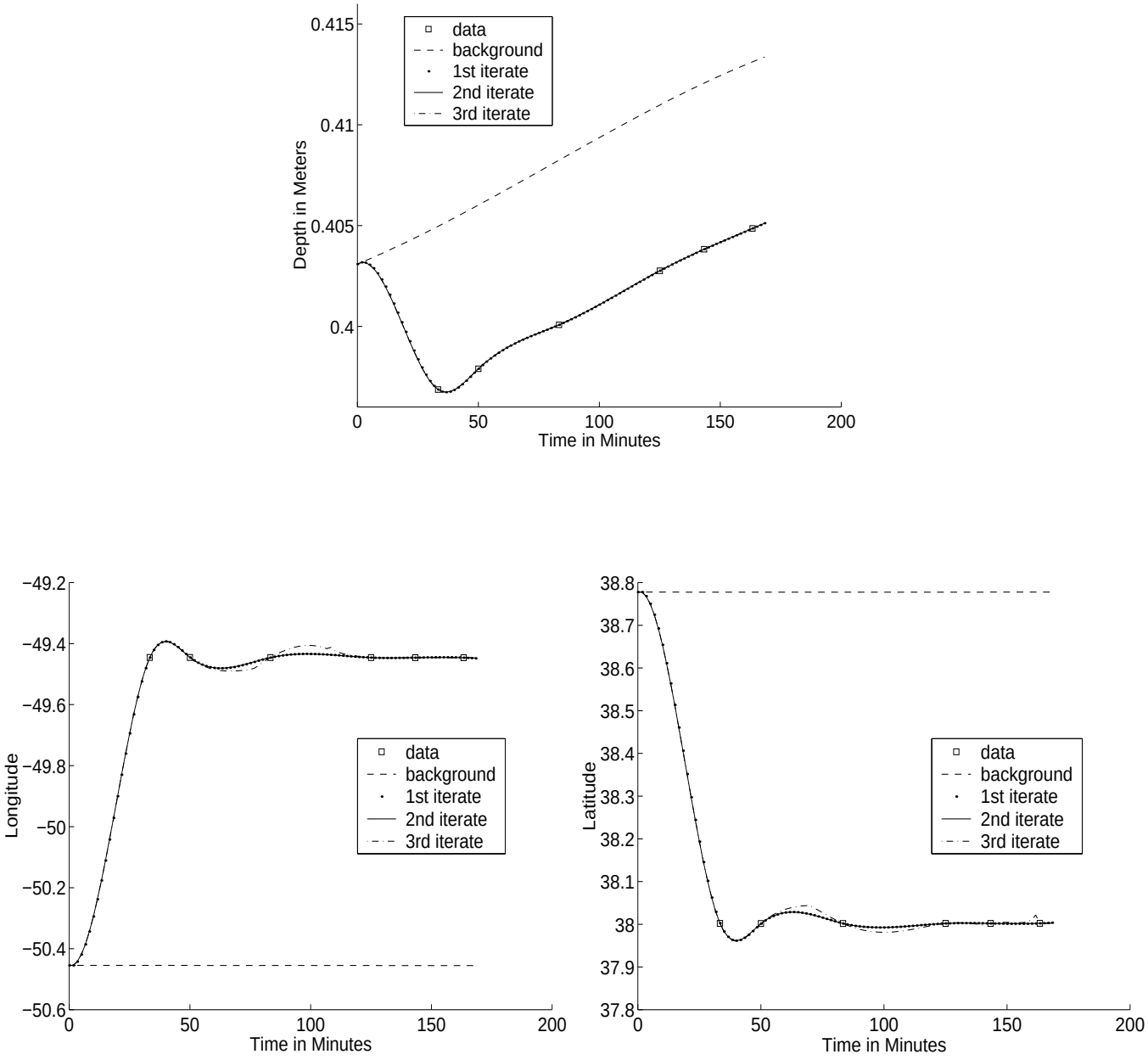

Figure 8: Time series convergence of float with initial position -50.45° longitude, 38.78° latitude. The equivalent depth, longitude or latitude is given by the data at six different times (33, 50, 83, 125, 143 and 163 minutes) and assimilated into the model. The standard deviation of the data is 1% of the width of the domain, and the inverse weight in the dynamics is 25% of the accelerations.

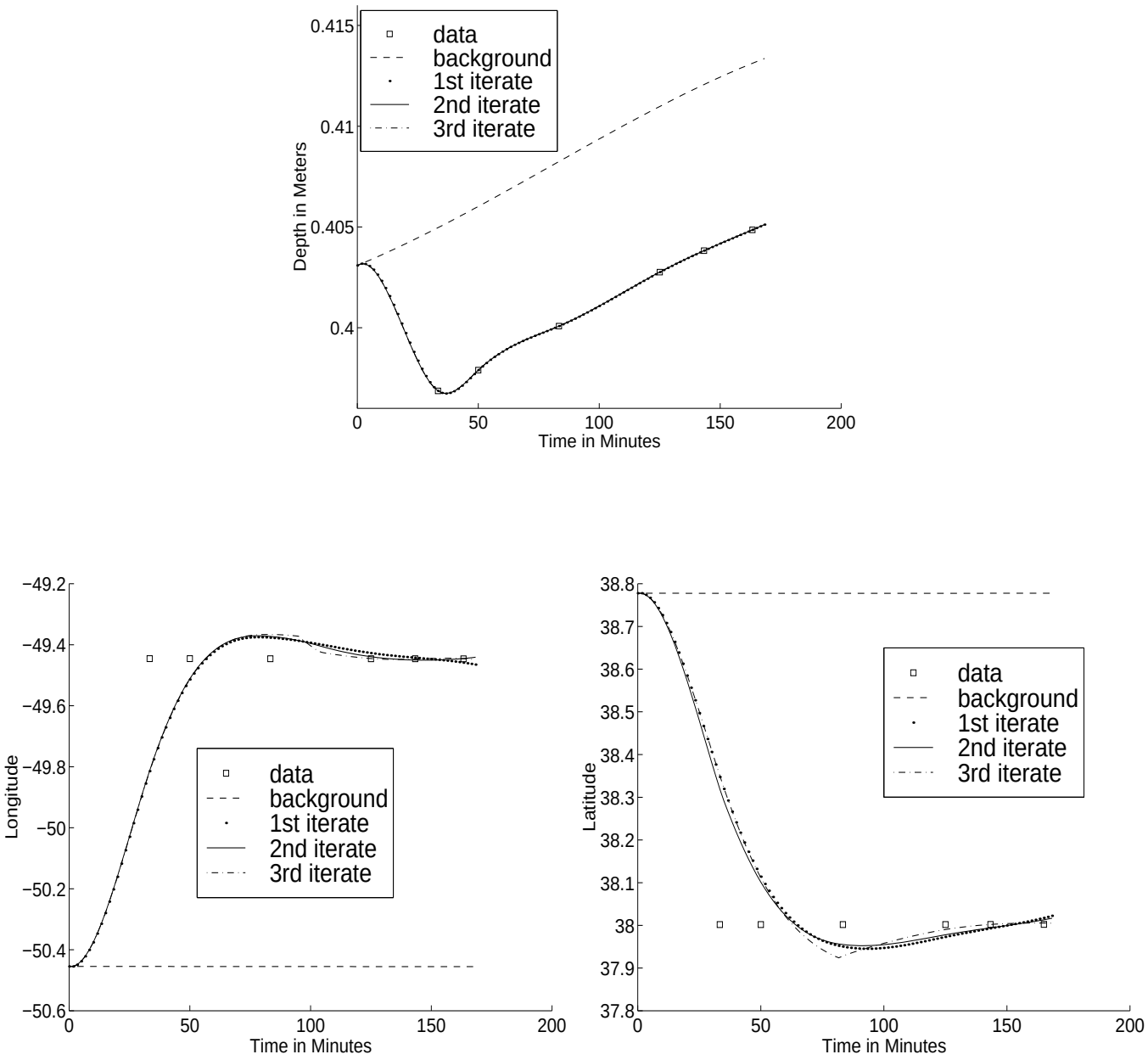

Figure 9: Time series convergence of float with initial position -50.45° longitude, 38.78° latitude. The equivalent depth, longitude or latitude is given by the data at six different times (33, 50, 83, 125, 143 and 163 minutes). The standard deviation of the data is 30% of the width of the domain, and the inverse weight in the dynamics is 10% of the accelerations.

Table 1: Numerical parameters and weights.

Time interval	$\triangle t$	100 s
Space interval	$\triangle\alpha, \triangle\beta$	$\pi/792$ rad, $\pi/810$ rad
Dynamical weight(25%)	$W_{f^\lambda}\triangle\alpha\triangle\beta\triangle t$	1×10^{12} $(\text{rad/s})^{-4}$
	$W_{f^\theta}\triangle\alpha\triangle\beta\triangle t$	1.8×10^{12} $(\text{rad/s})^{-4}$
Initial weight	$W_{I^{\lambda_t}}\triangle\alpha\triangle\beta$	2.5×10^{18} $(\text{rad/s})^{-2}$
	$W_{I^{\theta_t}}\triangle\alpha\triangle\beta$	5×10^{18} $(\text{rad/s})^{-2}$
Data weight(1%)	$\omega^\lambda\triangle\alpha\triangle\beta\triangle t = \omega^\theta\triangle\alpha\triangle\beta\triangle t$	6.25×10^4 rad^{-2}
	$\omega^h\triangle\alpha\triangle\beta\triangle t$	6.25×10^4 m^{-2}
Boundary weight	$W_b^{\lambda_w} = W_b^{\lambda_e} = W_b^{\theta_s} = W_b^{\theta_n}$	
	$W_b^{\lambda_w}\triangle\alpha\triangle t$	625 rad^{-2}
	$W_b^{h_w} = W_b^{h_e} = W_b^{h_s} = W_b^{h_n}$	
	$W_b^{h_w}\triangle\alpha\triangle t$	625 m^{-2}